Fluid-fluid and fluid-solid phase equilibria in carbon dioxide + waxy systems 1. CO + n-C

Jean-Luc Daridon, François Montel, Dan Vladimir Nichita, Jérôme Pauly

Fluid-fluid and fluid-solid phase equilibria in carbon dioxide + waxy systems 1. CO_2 + n-C_{17}

Jean-Luc Daridon[1,*], François Montel[1], Dan Vladimir Nichita[1], Jérôme Pauly[2]

1 Laboratoire des Fluides Complexes et leurs Réservoirs, LFCR, UMR 5150, Université de Pau et des Pays de l'Adour, E2S UPPA, CNRS, TOTAL, 64000 Pau, France

2 Total SA ; CSTJF Avenue Larribau, PAU Cedex 64018, France

Corresponding author : jean-luc.daridon@univ-pau.fr

Abstract

The objective of the present work is to investigate the full phase diagram of a binary system composed of carbon dioxide and a heavy paraffin. An alkane with an odd carbon number was chosen since mixtures of paraffins crystallize in the orthorhombic structure like pure odd paraffins do. The normal-heptadecane was taken into consideration for this study as it has a melting temperature close to the ambient condition (295 K). The work consists in measuring both fluid phase equilibria and fluid-solid phase transition conditions. The measurement of liquid-vapor and liquid - liquid phase transition in the temperature range 273 - 363 K has been made as well as the measurements of solid crystallization up to 70 MPa. The influence of carbon dioxide content has been studied from 0 to 99%.

1. Introduction

Wax precipitation is one of the main issues of oil and gas flow assurance in cold and deep-water fields [1]. Dissolved in reservoir fluids under reservoir pressure and temperature

conditions, the high molecular weight paraffins are likely to precipitate out of solution and to deposit during oil production, transportation and storage. The deposition and buildup of solid waxes on the inner surface of the cold pipe wall decreases the pipeline cross-sectional area and increases the surface roughness of pipes causing a restriction of oil flow and ultimately plugs the production equipments. Mitigation and remediation of waxy solid requires use of various techniques which includes mechanical cleaning (pigging) [2], chemical injection (inhibitors, dispersants or solvent) [3], thermal method (insulation, heating) [4,5] and surface treatment (anti-wax coating) [6]. Most of these techniques are costly and must be expanded in right place upon in an adequate manner. The prediction of the location of potential problems related to wax deposition requires information about fluid-fluid and fluid-solid phase behavior of waxy reservoir fluids. For this purpose, the study about the influence of light components such as methane, ethane etc., are very important, since they change the solvation capacities of live oil when its pressure decreases.

To address the issue of the phase equilibria of such light-heavy parrafins asymmetric mixtures, experimental phase equilibrium measurements were carried out in previous works on C_1 + n-C_{17} [7] and C_1 + paraffin distributions [8-9]. In addition to methane, carbon dioxide can influence the phase behavior because it is naturally present in significant proportion in reservoir fluid such as crude oil from Brazilian pre-salt fields [10] or because it is injected [1] into oil fields to improve oil displacement by miscible or non-miscible CO_2 flooding so as to enhance oil recovery. The objective of the present work is to investigate the full phase diagram of a binary system composed of carbon dioxide and a heavy paraffin. An alkane with an odd number of carbon was chosen since mixtures of paraffins crystallize in the orthorhombic structure like pure odd paraffins do. The heptadecane was taken into consideration for this study as it has a melting temperature close to the ambient condition (295 K). The work consisted in measuring both fluid phase equilibria and fluid-solid phase transition conditions by a synthetic method. A total of 14 different mixtures with compositions of carbon dioxide ranging from 10 to 99% were investigated in such a way as to achieve plotting *p,x* phase diagram in addition to isopleths. The conditions of fluid-fluid phase transitions were determined from the wax appearance temperature to 363 K whereas the fluid – solid boundary was determined from atmospheric pressure up to 70 MPa.

2. Material and methods

*2.1. **Materials***

Carbon dioxide was purchased from LINDE with a nominal purity of 99.995%. Normal-heptadecane was obtained from Sigma-Aldrich with a purity of 99 mol %. Both components were used without any further treatment. Details on pure components are listed in Table 1.

2.2. Experimental technique

The technique considered to measure both fluid - fluid and fluid - solid phase transition is based on a synthetic method which avoid sampling of the phases. The experimental device, which was presented previously [7] is mainly composed of high pressure a variable volume cell with full visibility. The cell consists of a horizontal cylinder with a movable piston and closed on the front by a sapphire window. A second sapphire window is placed on a lateral wall of the cell. This window enables the illumination of cell through an optical fiber whereas the front window allows a visual observation of the phases transitions occurring into the fluid thanks to a video camera mounted on an endoscope. The temperature of the fluid inside the cell is controlled by circulating a heat-carrier fluid thought three flow lines managed in the cell wall and connected to an external refrigerated and heating circulators suitable for temperature ranging from 263 to 293 K with a temperature stability of 0.01 K. The temperature is measured with an uncertainty of ±0.02 K by means of a calibrated Pt100 probe inserted inside the cell and connected to a high-precision thermometer. The pressure is changed by moving the piston manually. It is measured by a piezoresistive silicon pressure transducer (Kulite) placed inside the cell in order to reduce the dead volume. As this pressure transducer is subject to the same temperature changes than the fluid, it must be calibrated as a function of temperature. This calibration was done with an accuracy better than 0.02% in the full temperature and pressure range using a dead weight gauge (Budenberg brand).

Applying the synthetic method, the problem of sampling and analyzing phase in equilibrium is substituted by the difficulty of synthesizing the global mixture and by detecting phase changes. With regard to the first point, the mixtures were directly prepared in the measuring cell by adding separately the liquid and gas components in the cell and by weighing them during injection. The n-heptadecane is first loaded into the cell by vacuum suck up. The n-heptadecane mass introduced during this operation is determined by weighing by means of precision balance. The carbon dioxide initially charged in an aluminum tank with a high capacity and fixed on a high weight / high precision balance is then added under pressure. Because of the high capacity of the aluminum tank in comparison to the amount of gas

transferred, the pressure remains constant in the reservoir tank as well as in the connecting tube during gas injection. Therefore, the amount of gas transferred is directly obtained by weighing the reservoir tank during filling. From this method of sample synthesis, the expended uncertainties in mass introduced were estimated to be better than 0.01 g for n-C_{17} and 0.005 g for CO_2. The resulting combined standard uncertainty in the global mole fraction z_{co2} is obtained from following relation:

$$u_c(z_{co2}) = z_{co2}(1 - z_{co2})\left(\frac{u^2(m_{co2})}{m_{co2}^2} + \frac{u^2(m_{c12})}{m_{c12}^2}\right)^{1/2} \quad (1)$$

Homogenization of the mixture after injection of the pure component into the cell is achieved with a Teflon-coated magnetic stirrer driven by a rotating magnetic system mounted externally to the cell.

With regards to the second point, a direct visual observation of phase changes was used to determine phase boundary. The usual synthetic method that consists in observing the appearance of new phases do not exactly give the phase envelope but a point just below as a certain amount of the new phase formed is needed to be observable [11]. To circumvent this problem, a bracketing strategy was used here. It consists first in observing the formation of a new phase by gradually changing either the temperature or the pressure conditions and then reversing the direction of this variation in a stepwise fashion so as to detect the disappearance of the last phase formed. The procedure is repeated several time by reducing the increment.

As long as the absolute value of the slope of the phase change is small in the *p,T* diagram, measurements can be performed by changing pressure along an isothermal process so as to determine p^{obs}. This concerns the liquid - vapor phase transition ($L + V \rightarrow L$) and the boundary between three-phase liquid - liquid and two-phase liquid – liquid domain ($L + L + V \rightarrow L + L$). On the contrary, for phase changes with a steep slope such as transitions from single liquid phase to either liquid – liquid ($L + L \rightarrow L$) or liquid – solid two-phase equilibrium ($L + S \rightarrow L$), measurements shall be taken at fixed pressure by changing temperature up to obtain T^{obs}. Using this method, the standard uncertainties in phase change observations are $u(p^{obs}) = 0.02$ MPa for liquid-vapor pressure and $u(T^{obs}) = 0.2$ K for both of liquid-liquid and liquid – solid phase transitions. These uncertainties come in addition to the uncertainty of pressure $u(p^{gauge})$and temperature $u(T^{gauge})$ gauges as well as in mixture composition. Therefore, in accordance to the Guide to the expression of Uncertainty Measurement (GUM) of the National Institute of

Standards and Technology [12], the uncertainties in either transition pressure $p^{LV\to L}$ and temperature $T^{LL\to L}$ (or $T^{LS\to L}$) measured respectively during and isothermal or an isobaric process correspond to the following quadratic sums:

$$u^2(p^{LV\to L}) = u^2(p^{gauge}) + u^2(p^{obs}) + \left[\left(\frac{\partial p^{LV\to L}}{\partial T}\right)u(T^{gauge})\right]^2 + \left[\left(\frac{\partial p^{LV\to L}}{\partial x_{co2}}\right)u(x_{co2})\right]^2 \quad (2)$$

$$u^2(T^{LL\to L}) = u^2(T) + u^2(T^{obs}) + \left[\left(\frac{\partial T^{LL\to L}}{\partial p}\right)u(p^{gauge})\right]^2 + \left[\left(\frac{\partial T^{LL\to L}}{\partial x_{co2}}\right)u(x_{co2})\right]^2 \quad (3)$$

where the derivative with respect to pressure, temperature and composition were obtained from numerical derivation of the full set of data.

Because of the phase rule, the domain of coexistence of three phases in equilibrium has a degree of freedom of one. Therefore, measurement of the such monovariant domains by a synthetic method simply consists in putting the system in the equilibrium condition and in reading the values of both pressure and temperature gauges. In these circumstances, as there is no need to observe appearance (or disappearance) of a phase, the uncertainties in p^{obs} or T^{obs} are zero for such three phase equilibrium condition measurements:

3. Experimental results and discussion

The system was investigated on the basis of isoplethic measurements performed on several mixtures with mole percentages of carbon dioxide ranging from 10 to 99 % and for temperatures ranging from 280 to 370 K. The results are reported in Tables 2 and 3 for fluid – fluid phase transition. Table 2 correspond to measurements carried out at fixed temperature whereas Table 3 lists the data obtained along isobars. The *p,T* condition of fluid-solid transitions are summarized in Table 4. Finally, the three-phase and four phase equilibrium data are given in Table 5. The global composition z_{co2} was added to simply show along which isopleth the measurements were carried out. The values reported do not correspond to any of the phases in equilibrium. The three liquid - vapor - solid phase equilibrium conditions given in this table were determined by direct observation and checked by recording the intersection of the two-phase liquid - vapor and liquid - solid phase envelope. The quadruple point was also observed experimentally and its location has been checked by noting the point of intersection of the three-phase curves. In this table, L_1 represents the CO2- rich liquid whereas L_2 stand for the hydrocarbon-rich liquid phase and S_2 is the pure n-hetadecane solid.

From these data the isopleth diagrams that groups the fluid-fluid and fluid-solid phase transition were built. For an illustrative purpose, *p,T* diagrams are shown in Figs. 1-3 for three

different compositions characteristic of mixtures with low, medium and high CO_2 content. Fig.1 shows the isopleth corresponding to a global carbon dioxide content of 41%. It only combines the bubble point curve $(L_2 + V \rightarrow L_2)$, the transition line between liquid + solid and liquid domain $(L_2 + S_2 \rightarrow L_2)$ and a part of the three-phase equilibrium curves $L_2 + V + S_2$, $L_1 + V + S_2$ and $L_1 + L_2 + S_2$ as for this composition no liquid –liquid cloud points were observed before solid appears whatever the temperature and pressure of investigation. Similar phase diagram is plotted in Fig 2 for the mixture composed of 75 % carbon dioxide. This mixture corresponds to the first system investigated where liquid phase splitting occurs. Indeed, it can be seen in this figure that the bubble point curve split in two parts below 303 K. At low pressure, appearance of vapor takes place along the three-phase equilibrium line where vapor exists in addition to two liquid phases; one rich in CO_2 (L_1) and one rich in hydrocarbon (L_2). At high pressure the bubble point curve turns into a liquid - liquid cloud point curve $(L_1 + L_2 \rightarrow L_2)$. Because the quantity of gas present in this mixture is still limited, liquid – liquid phase separation occurs at temperature lower than the critical point of pure carbon dioxide whereas solid formation appears at slightly lower temperatures than the melting line of pure n-hetadecane. Consequently, both curves intersect at moderate pressure (25 MPa). Above, this pressure, solid precipitate out of the single liquid phase and data correspond to liquid + solid to liquid boundary $(L_2 + S_2 \rightarrow L_2)$. Just below the temperature of this transition, the CO2 concentration increases in the fluid phase and it becomes unstable $(L_2 + S_2 \rightarrow L_1 + L_2 + S_2)$. Therefore, the Liquid + Solid domain is extremely narrow and cannot not be experimentally observed. At the scale of the diagram, the curve seems to overlap the three phases $L_1 + L_2 + S_2$ equilibrium curve . Below this pressure, waxy solid appearance takes place along the three phases equilibrium curve $(L_1 + L_2 + S_2)$. This three-phase equilibrium curve ends at the lower pressure in a quadruple point Q_1 $(L_1 + L_2 + V + S_2)$ where it intersect the three-phase equilibrium curves: $L_1 + L_2 + V$ and $L_2 + V + S_2$. Comparable phase diagram was obtained in Fig 3 for the mixture with 85 % CO_2. The addition of carbon dioxide moves the bubble pressures towards higher pressures and it increase the temperature of liquid - liquid separation in comparison to those of Fig. 2. Finally, this leads to a translation of the solid precipitation curves towards low temperatures. As a result, solid formation only occurs in the two liquid phases domain and cloud point curve and wax appearance curve no longer cross. The location of the three-phase equilibrium line as well as the quadruple point remains unchanged in the *p,T* diagrams as their variances are equal to one and zero respectively according to the phase rule.

Figs. 4-7 are given to show the phases observed in the high pressure cell filled with a mixture with 85 % of carbon dioxide corresponding to the phase diagram given in Fig 3. The first picture (Fig. 4) shows the visual observation performed at the *p,T* conditions corresponding to three L_2 (at bottom) + L_1 (in the middle) + V (at the top) phases in equilibrium and identified in Fig. 3 by the open circle mark ○. Fig. 5, characterized by the plus sign ✚ symbol of Fig 3 shows the system in two liquid phases $L_1 + L_2$ equilibrium. The CO_2 rich phase (L_1) appears here at the bottom of the cell which reveals that the CO_2 rich phase have a higher density than the hydrocarbon rich phase. Consequently, a density inversion occurred by increasing pressure between condition of Figs. 4 and 5. Fig. 6 provides a picture of the cell taken under the three-phase equilibrium condition located by the triangular symbol ▲ in Fig. 3. It can be seen here that the waxy solid crystals are found at the top of cell dispersed in the least dense liquid phase. Finally, Fig. 7 depicts the observation of quadruple point Q_1 where pure S_2 is in equilibrium with three fluid phases : L_1, L_2, V (square symbol ■ in Fig.3). Again, waxy solids crystals remain in suspension in least dense liquid phase in the middle of the cell. Because of the phase rule, the domain of coexistence of four phases in equilibrium has a degree of freedom of zero. Therefore, measurement of the such invariant point simply consists in reading the values of both pressure and temperature when four phases are observed in equilibrium in the measurement cell.

The solid-fluid transitions measured in the different mixture were plotted in the same graph in Fig. 8. Below 75% of carbon dioxide the solid–fluid boundary curves start from the three-phase $L_2 + V + S_2$ equilibrium curve. It can be observed in this figure that the solid–liquid boundary curves appear nearly linear and all parallel to the three-phase $L_1 + L_2 + S_2$ equilibrium line meaning that the dissolution of carbon dioxide in the heavy paraffin lead to temperature drop independent of pressure in this pressure range. Moreover, by plotting the change in temperature caused by addition of carbon dioxide in n-heptadecane at a given pressure above the pressure of quadruple point Q_1 (Fig. 9), it can be seen that temperature drop of solid appearance increases linearly with CO_2 content with of average rate of - 0.20 K/CO_2 mol% up to 75%. Above this composition corresponding to the beginning of liquid-liquid phase separation and up to 97% solid crystals appear along the three-phase $L_1 + L_2 + S_2$ equilibrium line and the temperature drop of solid formation keeps constant due to the phase rule as observed in Fig 9. Above 97% the solid–fluid boundary curves shift again to the low temperatures. For these high CO_2 content mixtures solid–fluid boundary curves start from the

three-phase $L_1 + V + S_2$ equilibrium curve located at lower temperature than quadruple point Q_1.

As for fluid-solid transitions, the fluid-fluid phase transitions measured in the different mixtures are gathered in the same graph in Fig. 10 where bubble point curves are characterized by solid symbols whereas hollow symbols are used for dew points. It can be noted from this figure that liquid –liquid phase separation appears at low temperature (below 305 K in the pressure range investigate) in mixture ranging from 75 to 97% of carbon dioxide. The liquid – liquid phase separation appears in continuity to the liquid-vapor transition curve that present a pressure minimum in addition to a maximum in pressure at higher temperature that those covered by the experiments. At high pressure (and low temperature) these cloud point curves have a positive slope with a high value whereas at lower pressure (and low temperature) the slope is negative. As a result, the fluid-fluid phase transition curves of these mixture pass by a minimum in temperature. The bubble point curve corresponding to 90% of carbon dioxide mol% merges with the dew points curve of the mixture containing 95%. This means that the critical points are located between these two phases boundary curves in the studied composition range. It is therefore possible to use these data to characterize the critical loci in the *p,T* projection of the phase diagram of the full binary system CO_2 + n-C_{17} given in Fig. 11. As can be seen in this figure a very good agreement was observed between these fluid-fluid phase boundaries and the critical line reported by Scheidgen [13].

The *p,T* projection of the phase diagram shown in Fig. 11 is a characteristic of type III according to the classification of van Konynenburg and Scott [14]. This type of systems discussed in detail by Quifiones-Cisneros [15] is characterized the separation of the critical loci in two discontinuous branches caused by the interaction of the liquid-liquid critical line $(L_2 = L_1)$ with the liquid-vapor critical line $(L = V)$. The lower branch in terms of temperature $(L_1 = V)$ begins at the critical point of pure CO_2 and ends in an upper critical end point $\big((L_1 = V) + L_2\big)$ where a liquid-vapor critical phase $(L_1 = V)$ is in equilibrium with a non-critical n-heptadecane-rich liquid phase L_2. The temperature of the UCEP differs from the critical temperature of pure CO_2 by only 2.8 K more making this critical branch extremely limited. The second branch of the critical loci begins at high temperature at the critical point of pure n-C_{17} and passes through a maximum followed by a minimum in pressure and finally diverge toward high pressures by passing through a minimum in temperature.

At quadruple point Q_1 , four three-phase lines intersect. It can be seen in Fig. 12 that the three-phase curve $L_1 + L_2 + V$ stretches from the ordinary quadruple point $L_1 + L_2 + V + S_2$ to the UCEP while remaining very close to the saturation curve of the carbon dioxide whatever the temperature. The second three-phase line ($L_1 + L_2 + S_2$) begin at the ordinary quadruple point and rises with a positive slope to high pressure. As its slope (5.35 MPa.K^{-1}) is higher than the those of the critical curve ($L_2 = L_1$) at high pressure (4.9 MPa.K^{-1} at 100 MPa), it seems that both curve will not intersect in a critical endpoint in which the pure solid S_2 phase should be in equilibrium with a critical fluid phase ($L_2 = L_1$). As a result, the $L_1 + L_2 + S_2$ line should extend indefinitely to high pressure. The third three-phase curve ($L_2 + V + S_2$) stretches with a negative slope from the quadruple point to the triple point of n-heptadecane. However, as observed on the in the *P*,*T*-projection of the phase diagram these three-phase curve intersect the solid–solid equilibrium line of pure carbon dioxide. This line delimits the order–disorder transition from the low temperature solid phase (orthorhombic phase β_0) to the high temperature phase (orthorhombic phase with a rotator state $\beta - RI$) [16]. Consequently, at this condition two solid phases are in equilibrium with the liquid and vapor leading to the existence of a second quadruple point Q_2 $\left(L_2 + V + S_{2,\beta 0} + S_{2,\beta - RI}\right)$. The *P*–*T* coordinates of this quadruple point can be obtained graphically in Fig. 12: $T_4 = 285.15$ K, $P_4 = 3.4$ MPa. As already noted by Flöter et al. [17] for methane + tetracosane and by Pauly et al. [7] methane+ n-hetadecane binary system, the existence of this solid-solid transition does not change the general shape of the three-phase equilibrium curve. Finally, the fourth three-phase curve ($L_1 + V + S_2$) runs from Q_0 to a third quadruple point Q_3 where two pure solid phases S_1 and S_2 are in equilibrium with liquid and vapor phases. The $L_1 + V + S_2$ curve keeps close to the carbon dioxide vapor pressure curve in extension to the three-phase curve $L_1 + L_2 + V$. This third quadruple point appears at a temperature below the ordinary triple point of pure carbon dioxide, at a lower temperature than those covered by the experiments. However, by incorporating pure carbon dioxide melting line in the low temperature region it become possible to draw schematically the full fluid-solid phase behavior in P, T projection of the phase diagram. The result shown in Fig. 13 looks like a type E according to the classification proposed by Yamamoto et al. [18] although it differs slightly from the latter due to the absence of a second critical end point.

Using the raw isoplethic data of the form (T_i, p_i) for a given phase transition and a smoothing function, it was possible to derive cross-sections by linear regressions. As no

theoretical functional form exists for representing both the fluid and solid phase envelopes, empirical approximation functions with few parameters a_j were used to regress raw data. However, since the fitted function plays an essential role for the goodness of the fit but also, and perhaps most importantly, for the suitability of the interpolation, five different approximation functions of the form $p_l^{tr} = f_l(T, a_j)$ were independently fitted for each transition *tr*. A linear least squares regression was employed to determine the fitted parameter a_j as well as the matrix of covariance σ_{ajak}^2 between two parameters [19] corresponding to:

$$\sigma_{ajak}^2 = \sum_{i=1}^{n_{data}} \left(\frac{\partial f_l}{\partial a_j}\right)\left(\frac{\partial f_l}{\partial a_k}\right) u^2(p_i) \quad (4)$$

where n_{data} is the number of experimental data for a given isopleth. The obtained parameter were used to calculate an estimation of the phase change pressure p_l^{tr} whereas the uncertainty $u^2(p_l^{tr})$ associated with this estimation was calculated from the covariance matrix.

According to the propagation law recommended by the GUM [12] when some of the input quantities are correlated, it takes the following form:

$$u^2(p_l^{tr}) = \sum_{j=1}^{n_{para}} \left(\frac{\partial f_l}{\partial a_j}\right)^2 \sigma_{aj}^2 + 2\sum_{j=1}^{n_{para}-1} \sum_{k=j+1}^{n_{para}} \left(\frac{\partial f_l}{\partial a_j}\right)\left(\frac{\partial f_l}{\partial a_k}\right) \sigma_{aj}^2 \quad (5)$$

Finally, after repeating the operation with 5 different functions, the overall interpolated value and it uncertainty was estimated by calculating the mean and the variance of the mixture model by considering an unweight mixture of normal distribution as follows:

$$p^{tr} = \frac{1}{5}\sum_{l=1}^{5} p_l^{tr} \quad (6)$$

$$u^2(p_l^{tr}) = \frac{1}{5}\sum_{l=1}^{5} \left(u^2(p_l^{tr}) + p_l^{tr\,2} - p^{tr\,2}\right) \quad (7)$$

The resulting (*P*, *x*) data at fixed temperature are listed in Tables 6 and 7 along with their expanded uncertainties. The isothermal phase diagrams constructed from these data are given in Figs. 14 and 15 for two isotherms below the UCEP (293.15 and 303.15 K).

The isotherm 293.15 K is ranged between the triple point of heptadecane and quadruple point Q_1 where three fluid phases L_1, L_2, V coexist with pure solid S_2. Therefore, it intersects the PT projection of the three-phase curve $(L_2 + V + S_2)$. As this temperature range between Q_1 and the UCEP it also intersects the $(L_1 + L_2 + V)$ three-phase line. Finally, as this temperature is close to Q_1, the isotherm crosses the projection of the three-phase $L_1 + L_2 + S_2$ equilibrium line at a pressure covered by the experiment. These intersections with the three phase equilibrium curves correspond to three horizontals in the *p*, *x* phase diagram according

to the phase rule as shown in Fig. 16. Finally, in the *p, T* projection of the phase diagram, the isotherm 293.15 K intersects the vaporization curve of pure carbon dioxide just above the $(L_1 + L_2 + V)$ three-phase line, whereas it cross the sublimation curve of pure n-heptadecane at low pressure. Consequently, in low CO_2 content range, the vapor-liquid equilibrium domain starts from the three phase equilibrium conditions, where the bubble point curve intersects the $L_2 + V + S_2$ horizontal whereas it ends in the high CO_2 content range at the boiling points of pure carbon dioxide, where the curve corresponding to the liquid phase intersects the curve that represents the vapor phase composition. At pressure higher than 5.7 MPa, liquid immiscibility occurs. It can be noticed that the two-liquid-phase domain is very little influenced by pressure. The almost vertical lines which delimit it lead to think that the domain is unclosed at high pressure but in fact the liquid-liquid domain is vanishing at higher pressures, since the heavy component goes entirely from the hydrocarbon-rich liquid phase to the solid phase at the three-phase $(L_1 + L_2 + S_2)$ equilibrium pressure.

The isotherm 303.15 K is higher than the triple point of pure heptadecane and still below the than the UCEP. Consequently, the liquid vapor curve in Fig. 15 starts at low pressure from the boiling point of n-heptadecane and ends at the boiling point of pure CO_2. At this temperature, the isotherm still intercepts the three-phase line between saturation vapor pressure curves of both pure components in the *p,T* projection of the phase diagram. The liquid- vapor curve in the p,x plane is therefore cut by a three-fluid-phase equilibrium line separating the vapor–liquid and liquid-liquid regions. As this temperature is lower than the minimum in the critical curve in the *p,T* projection (304.6 K) the liquid-liquid region is not ending with a critical point $L_1 = L_2$.

The two-liquid-phase domain which is not very sensitive to the influence of pressure seems running to infinite pressure but It should indeed end when it crosses the solid – liquid transition line at a pressure higher than experimental range. The other isotherms studied concerns temperature higher than the UCEP. The corresponding *p,x* phase diagram shown in Fig 16 is therefore a fairly classical diagram with a two-phase equilibrium curves that merge in a $L_2 = V$ critical point. Because of the existence in Fig. 10 of a minimum in pressure around 310 to 320 K in the isopleths corresponding to feed compositions ranging between 75% and 95%, the isotherm 313.15 K crosses the others in this composition range in Fig. 10.

Few experimental studies were previously carried out to study the phase behavior of the binary system CO2 - n-heptadecane. Vapor-liquid equilibrium and critical points were

measured by Pohler [20] between 323.15 and 393.15 K, whereas Scheidgen [13] reported the *p,T* critical curve between 304.6 and 393.15 and pressures up to 100 MPa. Both Liquid – solid and Liquid-liquid-vapor phase equilibria were not observed in these previous experiments. As shown in Figs 17 and 18 the VLE data in the present study deviates significantly from the ones reported by Pohler [20]. as shown in Figure 4. The lower the temperature the higher is the deviation between both sets of data. Nevertheless, it can be seen that the critical pressures given by Pohler [20] also deviates from those reported by Scheidgen [13]. These data are on the contrary very consistent with the present work as already noted in Fig. 11.

Conclusions

The phase behavior of the binary system made up of carbon dioxide and n-heptadecane was thoroughly investigated by measuring both fluid – fluid and fluid – solid phase transitions. From these measurements, the isopleth and p,x phase diagram were constructed.

ACKNOWLEDGMENTS

The authors would like to gratefully acknowledge Total that has provided financial support for our works on carbon dioxide + waxy systems from which this paper was written.

References

1. Zhenyu Huang, Sheng Zheng, H. Scott Fogler, Wax Deposition Experimental Characterizations, Theoretical Modeling, and Field Practices
2. Poole GL, Brock G, Szymczak S, Casey G. Successful pipeline cleanout: lessons learned from cleaning paraffin blockage from a deepwater pipeline; 2008H. Quinteros-Lama, F. Llovell, J. Supercrit. Fluids **111**, 151 (2016)
3. Fei Yang, Yansong Zhao, Johan Sjöblom, Chuanxian Li & Kristofer G. Paso (2015) Polymeric Wax Inhibitors and Pour Point Depressants for Waxy Crude Oils: A Critical Review, Journal of Dispersion Science and Technology, 36:2, 213-225

4. Wang, X., Qu, Q., Javora, P. H., Pearcy, R. G. (2009, February 1). New Trend in Oilfield Flow-Assurance Management: A Review of Thermal Insulating Fluids. Society of Petroleum Engineers. doi:10.2118/103829-PA
5. Danilović DS, Karović-Maričić VD, Čokorilo VB. Solving paraffin deposition problem in tubing by heating cable application. Therm Sci. 2010;14(1):247–53.
6. Jie Bai1 · Xu Jin2 Jun‑Tao Wu Multifunctional anti‑wax coatings for paraffin control in oil pipelines Petroleum Science (2019) 16:619–631
7. Pauly, J., Coutinho, J., Daridon, J.-L. High pressure phase equilibria in methane + waxy systems. 1. Methane + heptadecane. Fluid Phase Equilibria **2007**, 255 (2), pp. 193-199.
8. Pauly, J., Coutinho, J.A.P., Daridon, J.-L. High pressure phase equilibria in methane+waxy systems. 2. Methane+waxy ternary mixture. Fluid Phase Equilibria **2010**, 297 (1), pp. 149-153.
9. Pauly, J., Coutinho, J.A.P., Daridon, J.-L. High pressure phase equilibria in methane+waxy systems. 3. Methane+a synthetic distribution of paraffin ranging from n-C 13 to n-C 22. Fluid Phase Equilibria **2012**, 313, pp. 32-37.
10. Pauly, J., Coutinho, J. A. P., Daridon, J. L. High pressure phase equilibria in methane +waxy systems 1. Methane + heptadecane. *Fluid Phase Equilib.* **2007**, 255, 193–199.
11. Deiters, U. K.; Schneider, G. M. High Pressure Phase Equilibria: Experimental Methods. *Fluid Phase Equilib.* **1986**, 29, 145-160.
12. Taylor, B. N.; Kuyatt, C. E. Guidelines for Evaluating and Expressing the Uncertainty of NIST Measurement Results. NIST Technical Note 1297. U.S. Department of Commerce: Washington, DC, **1994**.
13. A. Scheidgen, Fluidphasengleichgewichte bin¨arer und tern¨arer Kohlendioxidmischungen mit schwerfl¨uchtigen organischen Substanzen bis 100MPa. Ph.D. Dissertation, Ruhr-Universit¨at Bochum, Bochum, 1997.
14. P.H. van Konynenburg, R.L. Scott, Critical lines and phase equilibria in binary van der Waals mixtures, Phil. Trans. Roy. Soc. London, Ser. A 298 (1980) 495-540.
15. Quifiones-Cisneros S.E., Phase and critical behavior in type III phase diagrams, Fluid Phase Equilib. 134 (1997) 103-112.
16. A. Würflinger, G.M., Schneider, Ber. Bun. Ges. Phys. Chem. 77 (1973) 121–128.
17. E. Flöter, Th.W. de Loos, J. de Swaan Arons, Fluid Phase Equilib. 127 (1997) 129–146

18. S. Yamamoto, K. Ohgaki, T. Katayama, Phase behavior of binary mixtures of indole or quinoxaline with CO2, C2H4, C2H6, and CHF3 in the critical region, The Journal of Supercritical Fluids 2 (1989) 63–72.
19. Numerical Recipes in FORTRAN 77: The Art of Scientific Computing W. Press, B. Flannery, S. Teukolsky, and W. Vetterling. *Cambridge University Press, 2 edition,* (*1992*)
20. H. Pöhler, Fluidphasengleichgewichte binärer und ternärer Kohlendioxidmischungen mit schwerflüchtigen organischen Substanzen bei temperaturen von 303K bis 393K und drücken von 10MPa bis 100MPa, Ph.D. Dissertation, Ruhr-Universität Bochum, Bochum, 1994.

Table 1.

Sample Description

Chemical Name	CAS	Source	Purity (mol fraction)	Purification Method
Carbon dioxide	124-38-9	Linde	0.99995	None
n-heptadecane	629-78-7	Sigma-Aldrich	0.99	None

Table 2

Pressure of Fluid-Fluid transition $p^{LV\rightarrow L}$ at a given temperature T in different mixtures of global composition $z_{co2} \pm U(z_{co2})$ in mol % with its expended (k=2) uncertainty $U(p^{LV\rightarrow L})$[a] .

T / K	$p^{LV\rightarrow L}$ / MPa	$U(p^{LV\rightarrow L})$ / MPa	T / K	$p^{LV\rightarrow L}$ / MPa	$U(p^{LV\rightarrow L})$ / MPa	T / K	$p^{LV\rightarrow L}$ / MPa	$U(p^{LV\rightarrow L})$ / MPa
$z_{co2} = 10.1 \pm 0.3$ %			$z_{co2} = 20.4 \pm 0.3$ %			$z_{co2} = 30.0 \pm 0.3$ %		
304.15	0.86	0.06	298.65	1.59	0.06	291.65	2.22	0.06
313.15	0.93	0.06	306.15	1.74	0.06	298.95	2.39	0.06
322.15	1.00	0.07	312.75	1.81	0.07	303.15	2.54	0.07
332.85	1.07	0.07	321.85	1.96	0.07	313.35	2.81	0.07
342.15	1.13	0.07	342.45	2.30	0.08	323.05	3.09	0.08
352.95	1.21	0.08	353.85	2.46	0.08	331.35	3.34	0.08
364.45	1.26	0.08	363.15	2.61	0.09	342.25	3.60	0.09
						354.95	3.95	0.1
						365.15	4.19	0.1
$z_{co2} = 41.3 \pm 0.2$ %			$z_{co2} = 49.8 \pm 0.2$ %			$z_{co2} = 60.3 \pm 0.2$ %		
304.75	3.68	0.06	285.65	3.30	0.05	284.95	4.1	0.05
314.05	4.11	0.07	290.85	3.68	0.05	287.75	4.3	0.05
323.45	4.59	0.07	301.75	4.38	0.06	293.25	4.79	0.05
332.95	4.92	0.08	313.25	5.09	0.06	302.65	5.63	0.05
345.55	5.48	0.08	323.15	5.68	0.07	312.85	6.57	0.06
354.85	5.88	0.09	329.65	6.13	0.07	322.85	7.52	0.07
361.85	6.16	0.10	343.15	6.92	0.08	335.15	8.7	0.07
			353.15	7.51	0.09	344.35	9.52	0.08
			363.65	8.21	0.10	353.05	10.2	0.08
						363.05	11	0.08
$z_{co2} = 68.9 \pm 0.1$ %			$z_{co2} = 75.1 \pm 0.1$ %			$z_{co2} = 80.2 \pm 0.1$ %		
283.35	4.20	0.05	293.55	7.66	0.05	300.55	16.41	0.08
292.55	5.23	0.05	299.95	6.77	0.05	301.95	15.10	0.08
301.05	6.20	0.05	303.05	7.32	0.05	302.65	14.60	0.08
313.95	7.95	0.05	309.15	8.16	0.06	303.55	14.10	0.08
323.15	9.24	0.06	313.45	8.81	0.06	304.55	13.49	0.08
332.65	10.57	0.06	325.25	10.93	0.06	305.55	13.09	0.08
342.85	11.79	0.06	333.85	12.43	0.07	307.05	12.46	0.08
352.65	12.88	0.06	342.65	13.53	0.07	308.45	12.27	0.08
361.95	14.00	0.07	352.55	14.63	0.07	310.55	12.22	0.08
			363.15	15.83	0.07	313.35	12.16	0.08
						319.85	12.95	0.07
						323.05	13.25	0.07
						331.45	14.44	0.07
						343.25	16.33	0.07
						351.55	17.42	0.07
						365.15	19.27	0.07

z_{co2} = 85.02 ± 0.05 %			z_{co2} = 90.04 ± 0.05 %			z_{co2} = 95.28± 0.05 %		
307.95	19.98	0.09	310.35	24.15	0.07	312.15	21.86	0.11
310.45	18.58	0.09	311.55	23.25	0.07	322.75	19.84	0.05
312.85	17.88	0.09	313.15	22.05	0.07	332.55	20.41	0.04
323.15	16.85	0.07	318.15	20.35	0.07	343.15	21.29	0.05
333.15	17.93	0.06	323.15	19.94	0.06	352.15	22.58	0.05
343.15	19.11	0.06	331.35	20.12	0.05	364.55	23.98	0.04
356.65	20.80	0.06	343.65	21.19	0.05			
361.65	21.50	0.06	352.25	22.28	0.05			
			363.15	23.62	0.05			
z_{co2} = 97.49± 0.05 %			z_{co2} = 99.00 ± 0.05 %%					
306.15	17.5	0.11	283.05	4.49	0.09			
310.15	16.59	0.10	292.65	5.98	0.09			
314.15	16.37	0.10	304.45	8.68	0.10			
323.15	17.15	0.10	315.15	11.35	0.10			
334.25	18.62	0.08	323.15	12.95	0.10			
343.15	19.7	0.08	333.15	15.24	0.08			
353.55	21.19	0.07	343.15	16.97	0.07			
363.55	22.49	0.06	353.15	18.41	0.07			
			363.15	19.22	0.08			

[a] Standard uncertainty *u* is *u*(*T*) = 0.1 K

Table 3

Temperature of Fluid-Fluid transition $T^{LL\to L}$ in different mixtures of global composition z_{co2} in mol% at a given pressure p with its expended (k=2) uncertainty $U(T^{LL\to L})$[a]

p / MPa	$T^{LL\to L}$ / K	$U(T^{LL\to L})$ / K	p / MPa	$T^{LL\to L}$ / K	$U(T^{LL\to L})$ / K	p / MPa	$T^{LL\to L}$ / K	$U(T^{LL\to L})$ / K
$z_{co2} = 75.1\%$			$z_{co2} = 80.2\%$			$z_{co2} = 85.0\%$		
25.93	286.95	0.53	55.94	295.15	0.48	68.93	302.25	0.45
12.91	287.15	0.53	47.91	294.85	0.47	49.89	301.15	0.45
8.85	289.75	0.53	26.4	294.85	0.47	28.37	302.05	0.45
			24.8	295.15	0.47	26.08	302.75	0.45
						24.28	303.95	0.45
						22.08	305.55	0.45
$z_{co2} = 90.0\%$			$z_{co2} = 95.3\%$			$z_{co2} = 97.5\%$		
57.49	304.75	0.45	59.89	304.95	0.45	69.96	297.55	0.51
38.84	305.05	0.45	52.47	304.75	0.45	35.87	297.65	0.51
32.14	306.25	0.45	33.84	305.15	0.45	30.18	298.15	0.51
29.05	307.15	0.45	28.85	306.15	0.45	25.39	299.15	0.51
26.85	308.15	0.45	25.86	307.55	0.45	22.90	300.15	0.51
25.35	309.15	0.45	23.56	309.55	0.45	20.20	302.15	0.51
						18.60	304.15	0.51

a Standard uncertainty u is u(p) = 0.02 MPa

Table 4

Temperature of Liquid-Solid transition $T^{LS\rightarrow L}$ in different mixtures of global composition z_{co2} in mol% at given pressure p^a.

p / MPa	$T^{LS\rightarrow L}$ / K	p / MPa	$T^{LS\rightarrow L}$ / K	p / MPa	$T^{LS\rightarrow L}$ / K	p / MPa	$T^{LS\rightarrow L}$ / K	p / MPa	$T^{LS\rightarrow L}$ / K
$z_{co2} = 10.1\%$		$z_{co2} = 20.4\%$		$z_{co2} = 30.0\%$		$z_{co2} = 41.3\%$		$z_{co2} = 49.8\%$	
10.87	295.45	12.40	294.45	5.19	290.15	4.89	287.75	5.68	286.25
19.91	297.35	21.41	296.35	21.41	293.75	9.86	288.85	12.41	287.55
21.61	297.65	29.88	298.15	35.88	296.95	23.41	291.65	23.41	289.85
29.38	299.65	39.87	300.15	49.90	299.65	29.99	293.25	35.88	292.55
39.86	301.95	50.08	302.25	58.92	301.65	41.89	295.65	49.71	295.45
54.48	305.05	69.89	306.25	69.41	303.85	51.92	297.65	60.45	297.65
69.86	308.55					60.94	299.45		
						69.93	301.55		
$z_{co2} = 60.3\%$		$zz_{co2} = 68.9\%$		$z_{co2} = 75.1\%$		$z_{co2} = 99.0\%$			
5.58	284.05	7.37	283.25	37.19	289.15	17.83	283.55		
7.86	284.35	8.85	283.65	58.06	293.15	27.97	285.15		
17.94	286.65	16.16	285.25	69.77	295.45	39.72	287.45		
26.91	288.55	26.52	287.45			49.13	289.15		
39.39	291.25	40.09	290.25			59.97	291.15		
52.63	294.05	50.62	292.45						
66.57	296.85	61.26	294.65						
		69.97	296.45						

a Standard uncertainty u is u(p) = 0.02 MPa and the combined expanded uncertainty Uc (k=2, level of confidence = 0.95) is $U(T^{LS\rightarrow L}) = 0.45$ K

Table 5

Three and four-phase *p, T* equilibrium conditions measured along different mixtures of feed composition z_{co2}.

T / K	p / MPa	z_{co2} mol%	T / K	p / MPa	z_{co2} mol%	T / K	p / MPa	z_{co2} mol%
$L_1 + L_2 + V$			$L_1 + V + S_2$			$L_1 + L_2 + S_2$		
282.55	4.39	90.0%	281.20	4.20	99.0%	282.55	4.39	90.0%
282.55	4.39	95.3%	$Q_1(L_1 + L_2 + V + S_2)$			282.55	4.39	282.55
283.45	4.51	80.2%	282.55	4.39	90.0%	282.75	4.51	80.2%
285.15	4.71	80.2%	282.55	4.39	95.3%	283.15	7.86	97.5%
285.15	4.69	90.0%	$L_2 + V + S_2$			283.65	10.22	283.65
285.15	4.69	95.3%	282.70	4.35	68.9%	283.75	10.94	85.0%
285.75	4.80	85.0%	283.60	4.00	60.3%	283.75	10.9	90.0%
287.35	4.96	80.2%	285.65	3.30	49.8%	285.35	18.77	95.3%
288.75	5.13	80.2%	287.00	2.71	41.3%	286.15	22.8	90.0%
290.05	5.25	75.1%	289.55	2.13	30.0%	286.25	23.94	97.5%
291.85	5.52	90.0%	291.75	1.50	20.4%	286.95	25.93	75.1%
291.85	5.52	95.3%	293.15	0.80	10.1%	287.15	28.42	80.2%
292.95	5.68	85.0%	294.65	0.10	10.1%	288.85	36.70	85.0%
293.35	5.69	97.5%				288.85	36.7	90.0%
294.95	5.96	80.2%				289.05	38.0	90.0%
296.45	6.21	80.2%				289.45	39.90	95.3%
296.75	6.20	90.0%				289.45	40.40	97.5%
296.75	6.20	95.3%				289.55	40.40	80.2%
297.25	6.25	97.5%				290.15	43.60	85.0%
297.75	6.41	90.0%				290.15	43.6	90.0%
297.75	6.41	95.3%				291.15	48.92	97.5%
300.75	6.81	80.2%				291.25	49.2	90.0%
300.75	6.84	97.5%				291.55	50.53	95.3%
301.45	6.90	90.0%				292.35	55.75	85.0%
301.45	6.90	95.3%				292.35	55.7	90.0%
302.25	6.99	97.5%				292.55	56.45	80.2%
302.95	7.15	80.2%				292.85	57.86	97.5%
303.15	7.17	85.0%				293.95	63.97	85.0%
304.55	7.37	85.0%				293.95	64.0	90.0%
304.65	7.45	80.2%				294.25	64.97	95.3%
305.95	7.62	85.0%				294.35	65.48	80.2%
306.45	7.71	85.0%				295.15	69.97	80.2%
306.75	7.74	90.0%				295.15	69.8	90.0%
306.75	7.74	95.3%						
306.85	7.74	80.2%						
306.95	7.74	85.0%						

a expanded uncertainty U (k=2, level of confidence = 0.95) are U(*T*) = 0.2 K and u(*p*) = 0.04 MPa

Table 6

Interpolated data of fluid-fluid transition pressure p with its expended (k=2) uncertainty $U(p)$.

z_{co2}	p	$U(p)$	p	$U(p)$	p	$U(p)$	p	$U(p)$
%	/ MPa	/ MPa	/ MPa	/ MPa	/ MPa	/ MPa	/ MPa	/ MPa
		293.15 K		303.15 K		313.15 K		323.15 K
10.1	0.79	0.05	0.86	0.03	0.93	0.03	1.00	0.04
20.4	1.52	0.04	1.67	0.03	1.83	0.04	1.99	0.04
30.0	2.25	0.04	2.53	0.03	2.81	0.04	3.09	0.04
41.3	3.06	0.04	3.58	0.03	4.07	0.04	4.54	0.04
49.8	3.81	0.03	4.45	0.03	5.08	0.03	5.71	0.03
60.3	4.80	0.02	5.72	0.03	6.63	0.03	7.54	0.03
68.9	5.34	0.03	6.62	0.03	7.90	0.03	9.18	0.03
75.1	7.70	0.04	7.19	0.04	8.98	0.03	10.62	0.03
80.2	-	-	14.33	0.05	12.24	0.05	13.44	0.04
85.0	-	-	24.90	0.07	17.70	0.07	16.85	0.07
90.0	-	-	-	-	22.11	0.06	19.85	0.06
95.3	-	-	-	-	21.40	0.05	19.82	0.05
97.5	-	-	19.44	0.05	16.37	0.05	17.28	0.05
99.0	6.55	0.06	8.91	0.05	11.09	0.05	13.10	0.06
		333.15 K		343.15 K		353.15 K		363.15 K
10.1	1.07	0.04	1.14	0.03	1.20	0.04	1.26	0.06
20.4	2.14	0.04	2.30	0.04	2.45	0.05	2.61	0.07
3.00	3.36	0.04	3.63	0.04	3.89	0.05	4.15	0.07
41.3	4.98	0.04	5.40	0.04	5.80	0.05	6.18	0.07
49.8	6.33	0.03	6.94	0.04	7.54	0.05	8.13	0.07
60.3	8.44	0.03	9.33	0.03	10.21	0.04	11.09	0.06
68.9	10.46	0.03	11.73	0.03	13.00	0.04	14.26	0.06
75.1	12.12	0.04	13.49	0.04	14.75	0.04	15.89	0.07
80.2	14.73	0.04	16.11	0.04	17.56	0.04	19.07	0.06
85.0	17.93	0.04	19.10	0.05	20.36	0.04	21.69	0.06
90.0	20.34	0.04	21.16	0.04	22.28	0.03	23.67	0.05
95.3	20.49	0.03	21.40	0.03	22.52	0.03	23.82	0.04
97.5	18.46	0.05	19.73	0.05	21.06	0.04	22.46	0.05
99.0	14.95	0.07	16.66	0.06	18.24	0.04	19.69	0.11

Table 7

Interpolated data of three phase equilibrium pressure and fluid-solid transition pressure p with its expended (k=2) uncertainty $U(p)$.

Transition/ Equilibrium	z_{co2} %	p / MPa	$U(p)$ / MPa	p / MPa	$U(p)$ / MPa
		293.15 K		303.15 K	
$L_2 + S_2 \rightarrow L_2$	10.1	-	-	45.6	1.4
	20.4	7.2	1.5	54.3	1.3
	30.0	18.7	1.3	66.2	1.7
	41.3	30.1	1.2	-	-
	49.8	38.9	1.5	-	-
	60.3	48.5	1.3	-	-
	68.9	53.9	1.2	-	-
	75.1	58.1	1.8	-	-
$L_1 + L_2 + V$	-	5.70	0.01	7.17	0.01
$L_1 + L_2 + S_2$	-	59.44	0.26	-	-
$L_2 + V + S_2$	-	0.80	0.06	-	-

Fig. 1. Isopleth phase diagram for the CO_2 – nC_{17} mixture with 41 mol% of CO_2. Black ●, bubble points $(L_2 + V \rightarrow L_2)$; red ▲, liquid–solid phase transitions $(L_2 + S_2 \rightarrow L_2)$; blue □, three-phase $L_2 + V + S_2$ equilibrium; blue Δ, three-phase $L_1 + L_2 + S_2$ equilibrium; blue ×, three-phase $L_1 + V + S_2$ equilibrium.

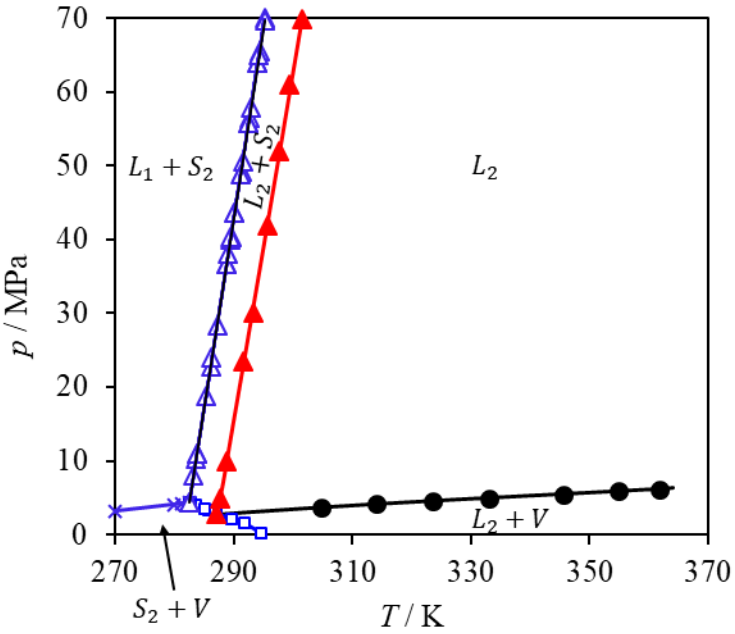

Fig. 2. Isopleth phase diagram for the CO_2 – nC_{17} mixture with 75 mol% of CO_2. Black ●, fluid-fluid phase transitions $(L_2 + V \rightarrow L_2)$ or $(L_1 + L_2 \rightarrow L_2)$; red ▲, liquid–solid phase transitions $(L_2 + S_2 \rightarrow L_2)$; blue ◇; three-phase $L_1 + L_2 + V$ equilibrium; blue □, three-phase $L_2 + V + S_2$ equilibrium; blue Δ, three-phase $L_1 + L_2 + S_2$ equilibrium; blue ×, three-phase $L_1 + V + S_2$ equilibrium.

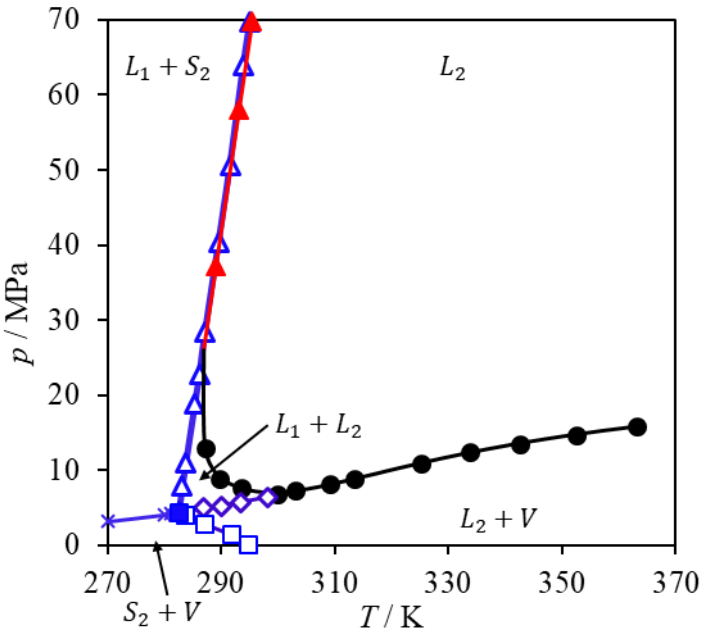

Fig. 3. Isopleth phase diagram for the CO_2 – nC_{17} mixture with 85 mol% of CO_2. Black ●, fluid-fluid phase transitions $(L_2 + V \rightarrow L_2)$ or $(L_1 + L_2 \rightarrow L_2)$; blue ◇; three-phase $L_1 + L_2 + V$ equilibrium; blue □, three-phase $L_2 + V + S_2$ equilibrium; blue Δ, three-phase $L_1 + L_2 + S_2$ equilibrium; blue ×, three-phase $L_1 + V + S_2$ equilibrium;; red ○, condition of observation shown of Fig. 4; +, condition of observation shown of Fig. 5; red ▲, condition of observation shown of Fig. 6; red ■, quadruple point $L_1 + L_2 + V + S_2$ shown in Fig. 7.

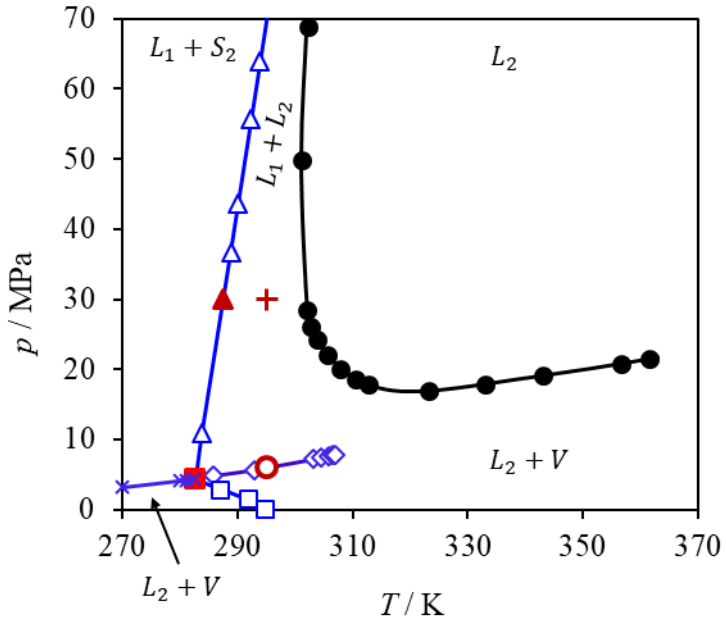

Fig. 4. Snapshots of the binary system with 85% of carbon dioxide observed in three-phase equilibrium ($L_1 + L_2 + V$) in the full visibility cell at temperature T = 295 K (⭕ mark in Fig. 3).

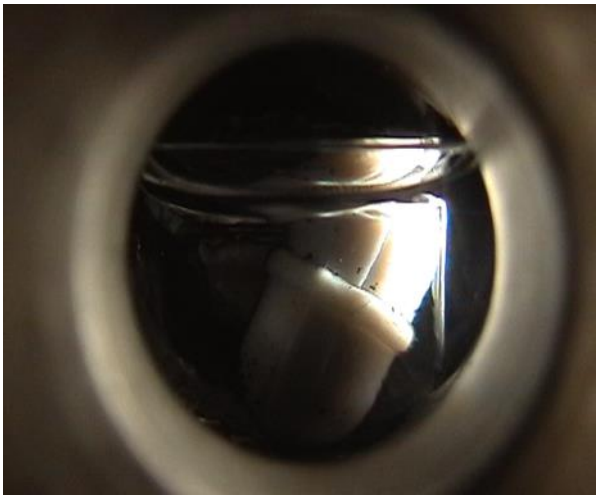

Fig. 5. Snapshots of the binary system with 85% of carbon dioxide observed in two phase equilibrium ($L_1 + L_2$) in the full visibility cell at temperature T = 295 K and pressure p = 30Mpa (✚ sign in Fig. 3).

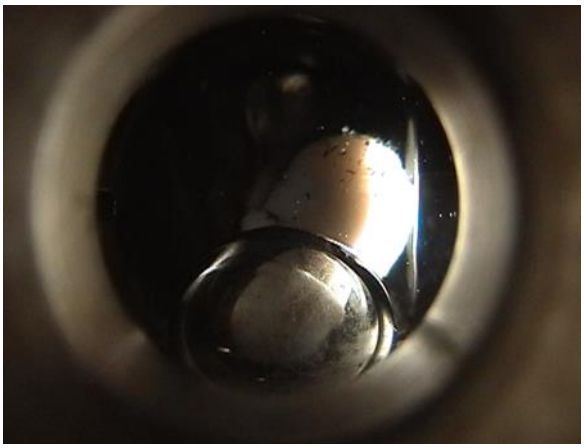

Fig. 6. Snapshots of the binary system with 85% of carbon dioxide observed in three-phase equilibrium ($L_1 + L_2 + S_2$) in the full visibility cell at pressure *p* = 30Mpa (▲ symbol in Fig. 3).

.

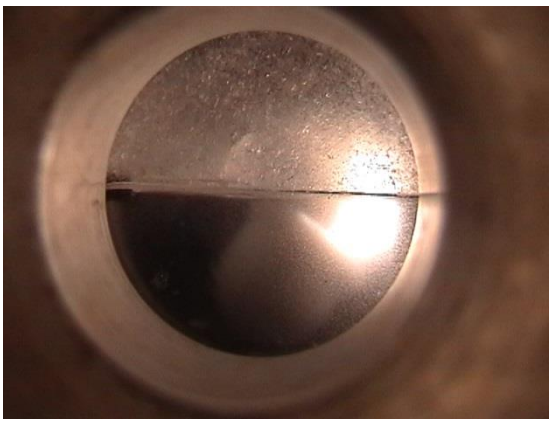

Fig. 7. Snapshots of the binary system with 85% of carbon dioxide observed at the quadruple point ($L_1 + L_2 + V + S_2$) (■ symbol in Fig. 3).

Fig. 8. Solid – fluid phase transitions measured in different mixtures. blue -, 10%; blue ●, 20%; blue ✳, 30%; blue ▲, 41%; blue–, 50%; ■, 60%; black ✕, 80%; black ●, 85%; black □, 90%; red ○, 95%; red △, 97.5%; red ◇, 99%; blue dotted line, three-phase $L_2 + V + S_2$ equilibrium.

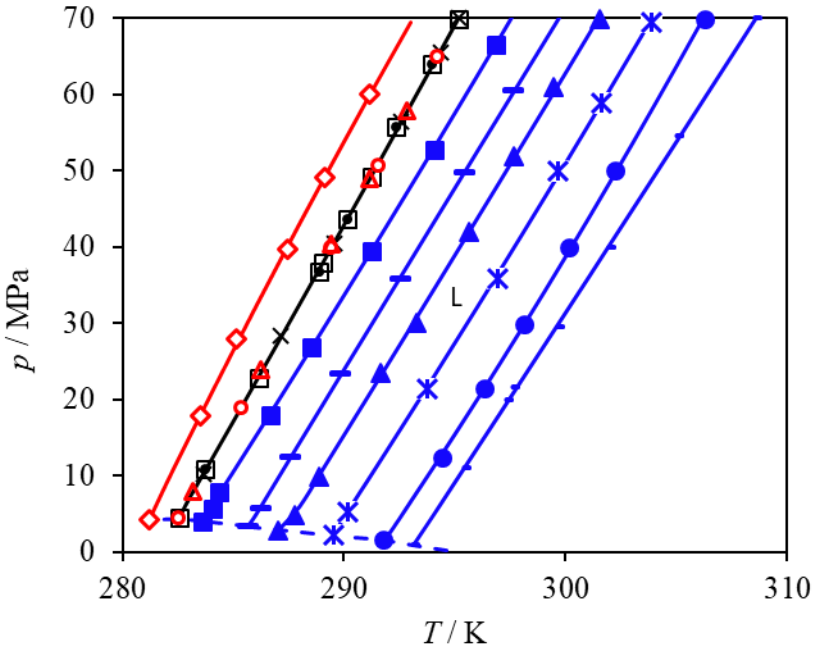

Fig. 9. Change ΔT in temperature of n-heptadecane crystallization caused by CO2 addition as a function of CO2 content in mol%.

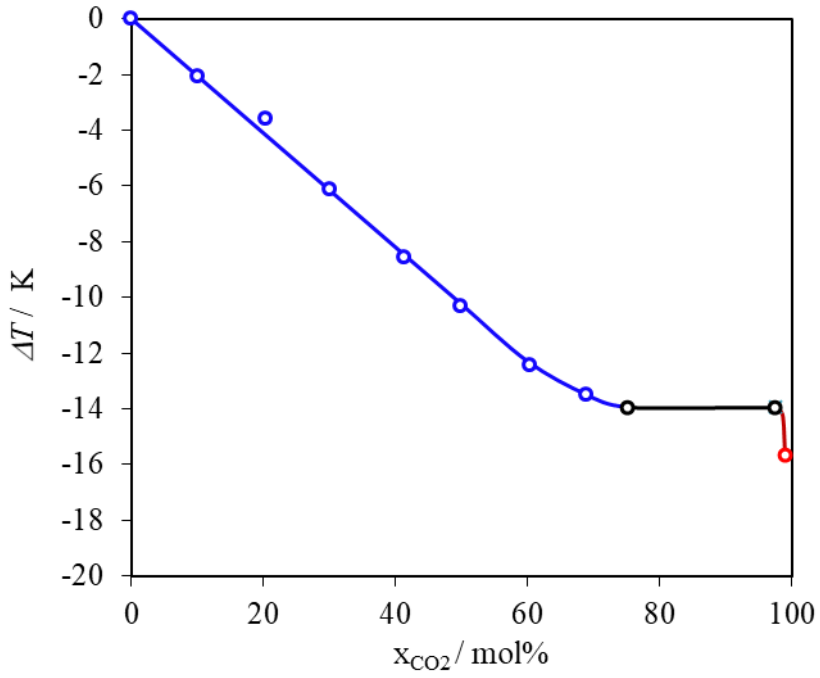

Fig. 10. Fluid – fluid phase transitions measured in different mixtures. blue ●, 20%; blue ▲, 41%; ■, 60%; ◆, 70%; black ✚, 75%; black ×, 80%; black •, 85%; black □, 90%; red ○, 95%; red Δ, 97.5%; red ◇, 99%; blue dotted line, three-phase $L_2 + V + S_2$ equilibrium; blue chain-dotted line, three-phase $L_1 + L_2 + S_2$

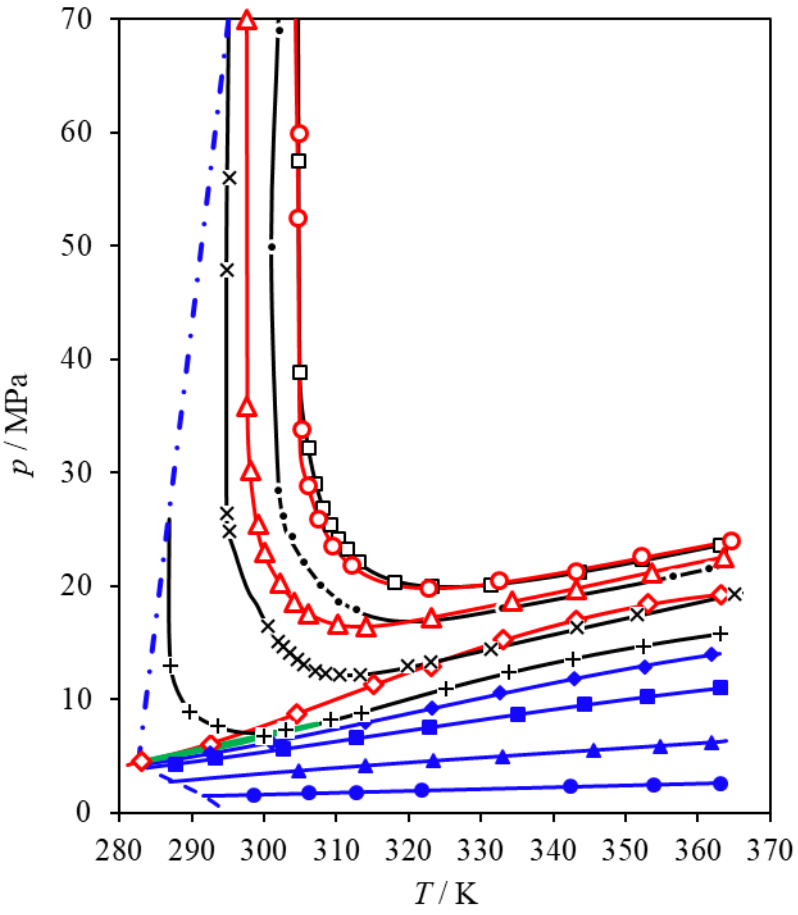

Fig. 11. *p,T* projection of the phase diagram in the experimental range. Blue □, three-phase $L_2 + V + S_2$ equilibrium; blue △, three-phase $L_1 + L_2 + S_2$ equilibrium; blue ◇, three-phase $L_1 + L_2 + V$ equilibrium; blue ×, three-phase $L_1 + V + S_2$ equilibrium; black ●, critical locus $L_2 = V$ or $L_2 = L_1$; black □, fluid phase envelope of isopleth 90%; red ○, fluid phase envelope of isopleth 95%; blue ●, UCEP; blue ■, quadruple point Q_1 $(L_1 + L_2 + V + S_2)$.

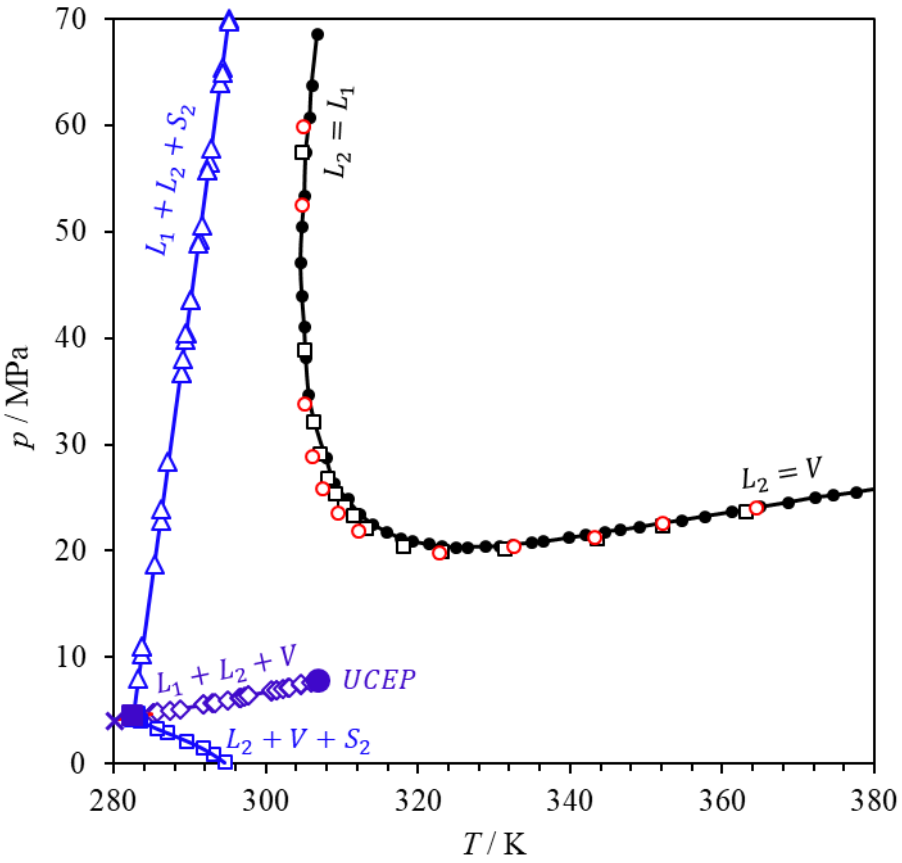

Fig. 12. Zoom of *p*,*T* projection of the phase diagram between the quadruple point and the UCEP. Blue □, three-phase $L_2 + V + S_2$ equilibrium; blue Δ, three-phase $L_1 + L_2 + S_2$ equilibrium; blue ◇, three-phase $L_1 + L_2 + V$ equilibrium; blue ×, three-phase $L_1 + V + S_2$ equilibrium; red ○, CO2 critical point; ●, UCEP; blue ■, quadruple points Q_1 and Q_2; red dashed line, CO2 vaporization pressure; green long-dashed line, n-C17 vaporization pressure; green dotted line, n-C17melting curve[13] ; green dot dash line, n-C17solid-solid transition curve [13].

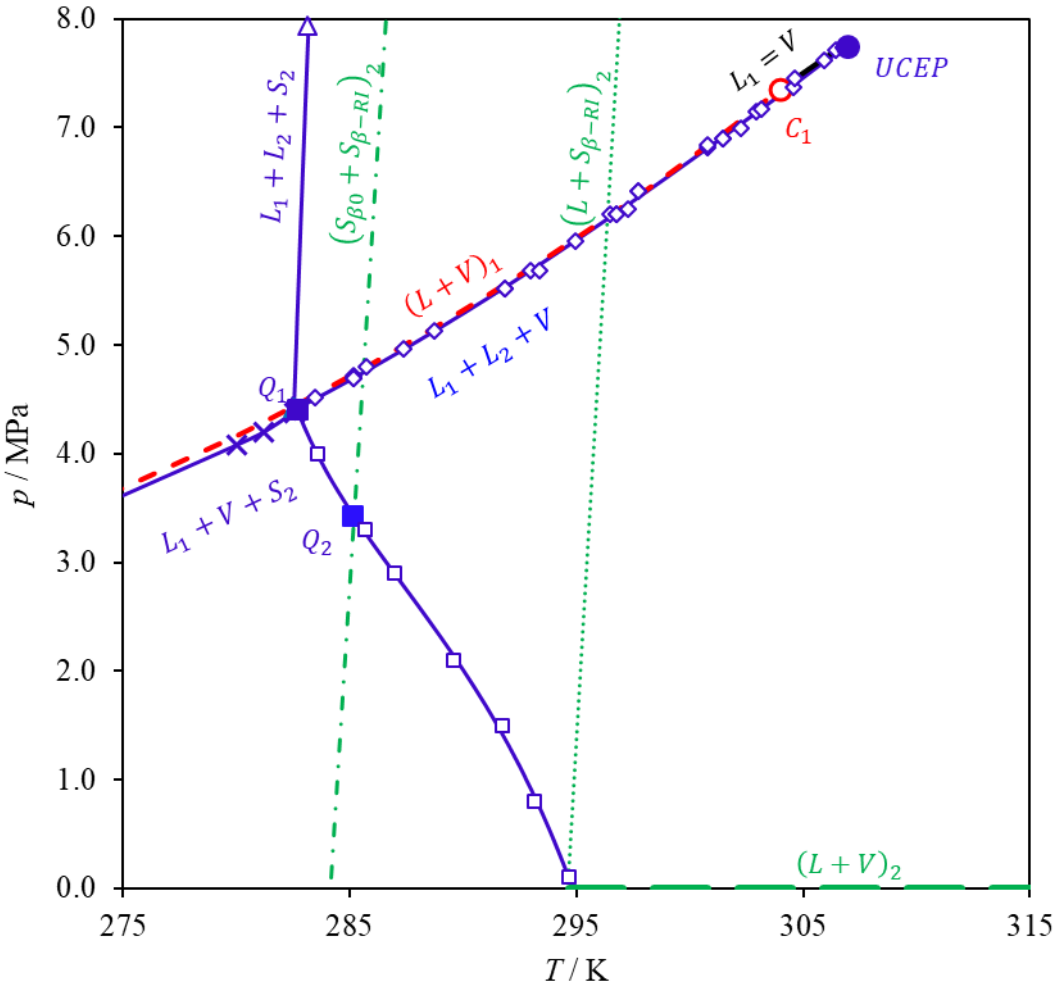

Fig. 13. *p,T* projection of the phase diagram . Blue solid line, three-phase equilibrium curves; black solid line, critical curve; blue solid lines, three-phase equilibrium curves ($L_1 + L_2 + V$, $L_1 + L_2 + S_2$, $L_2 + V + S_2$, $L_1 + V + S_2$); red ○, CO2 critical point; black ○, n-C17 critical point; ●, UCEP; blue ■, quadruple point Q_1 ; black Δ, quadruple point Q_2; blue ◆, quadruple point 3 ; black solid line, critical locus; red dash line, CO2 saturation curve; red dotted line, CO2 melting curve; green longdash line, n-C17 vaporization pressure; green dotted line, n-C17 melting curve [13] ; green dotdash line, n-C17solid-soli transition curve [13].

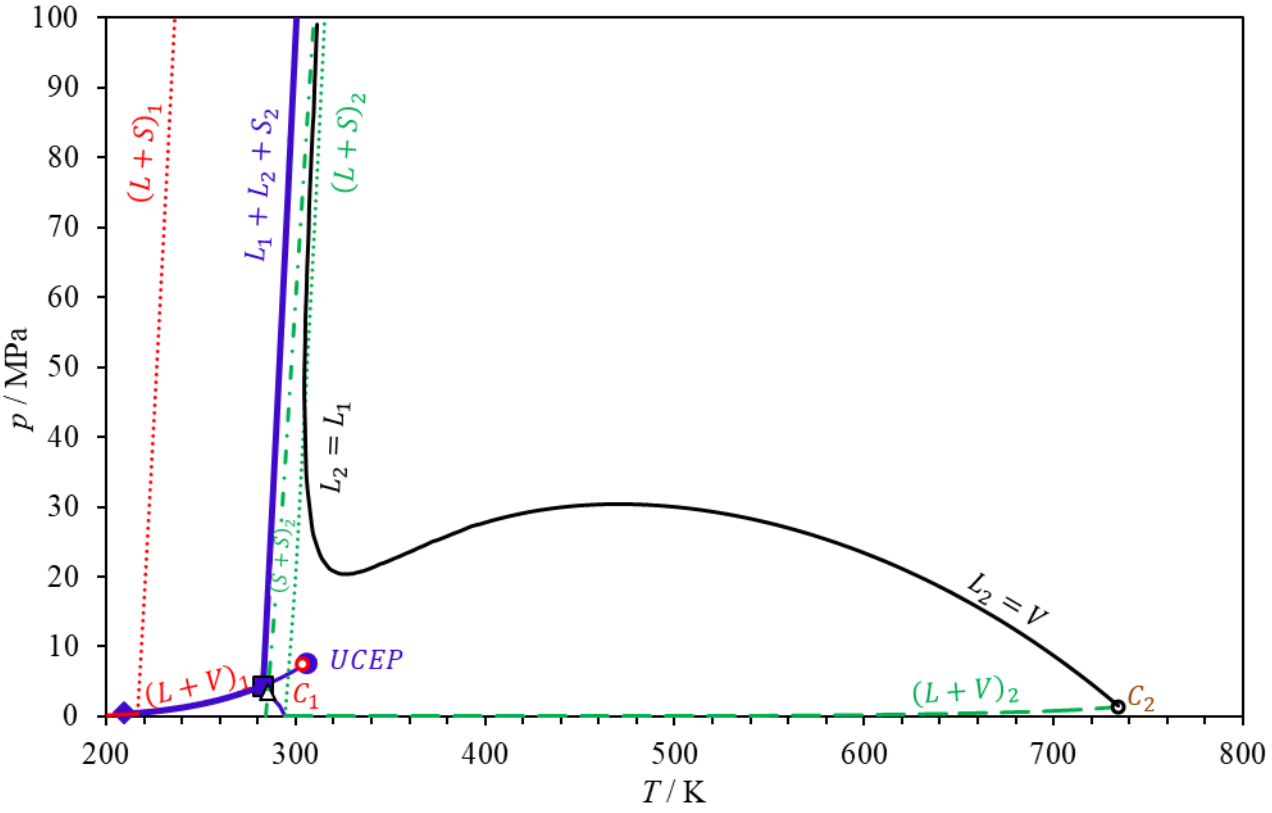

Fig. 14. Isothermal *p*,*x* phase diagram at T = 293.15 K. Black ●, fluid-fluid phase transitions $(L_2 + V \rightarrow L_2)$ or $(L_1 + L_2 \rightarrow L_2)$; green ×, fluid-fluid phase transitions $(L_1 + L_2 \rightarrow L_1)$; ; red ▲, liquid–solid phase transitions $(L_2 + S_2 \rightarrow L_2)$; red ■, liquid–solid phase transitions $(L_1 + S_2 \rightarrow L_1)$; blue ◇; three-phase $L_1 + L_2 + V$ equilibrium; blue □, three-phase $L_2 + V + S_2$ equilibrium; blue Δ, three-phase $L_1 + L_2 + S_2$ equilibrium.

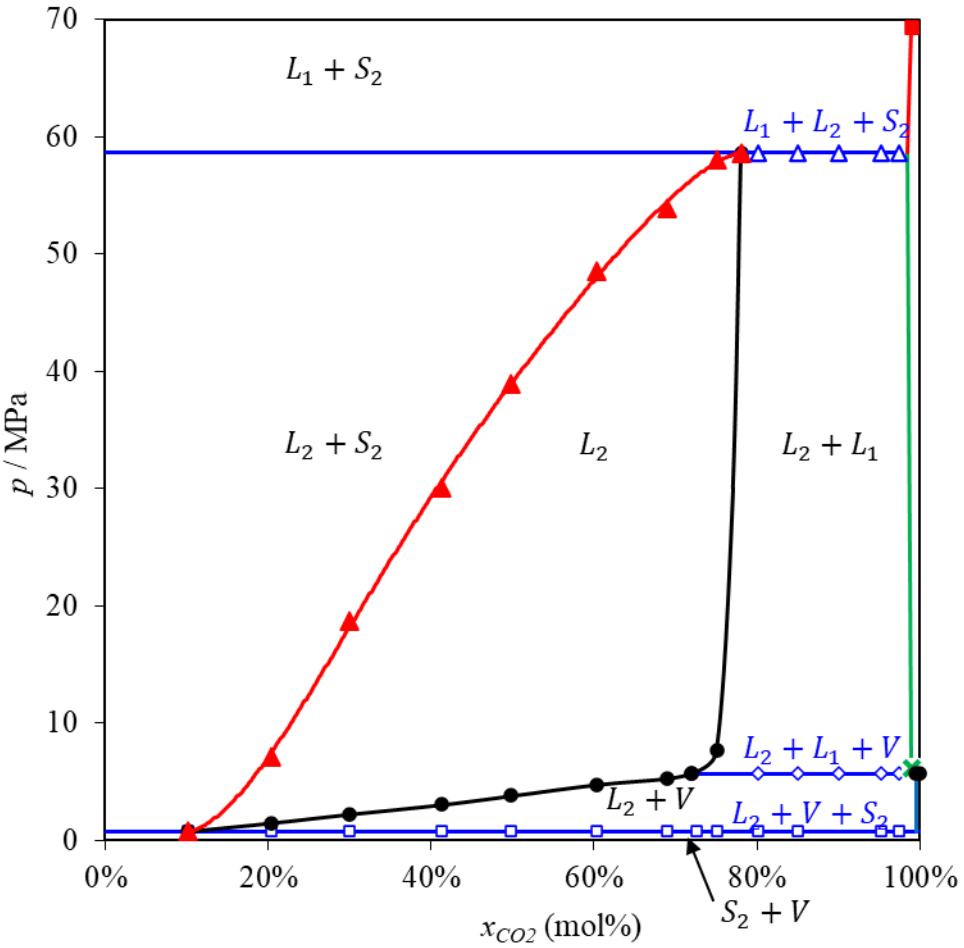

Fig. 15. Isothermal *p,x* phase diagram at T = 303.15 K. Black ●, fluid-fluid phase transitions $(L_2 + V \rightarrow L_2)$ or $(L_1 + L_2 \rightarrow L_2)$; green ×, fluid-fluid phase transitions $(L_1 + L_2 \rightarrow L_1)$; ; red ▲, liquid–solid phase transitions $(L_2 + S_2 \rightarrow L_2)$; blue ◇; three-phase $L_1 + L_2 + V$ equilibrium; blue □, three-phase $L_2 + V + S_2$ equilibrium; blue Δ, three-phase $L_1 + L_2 + S_2$ equilibrium.

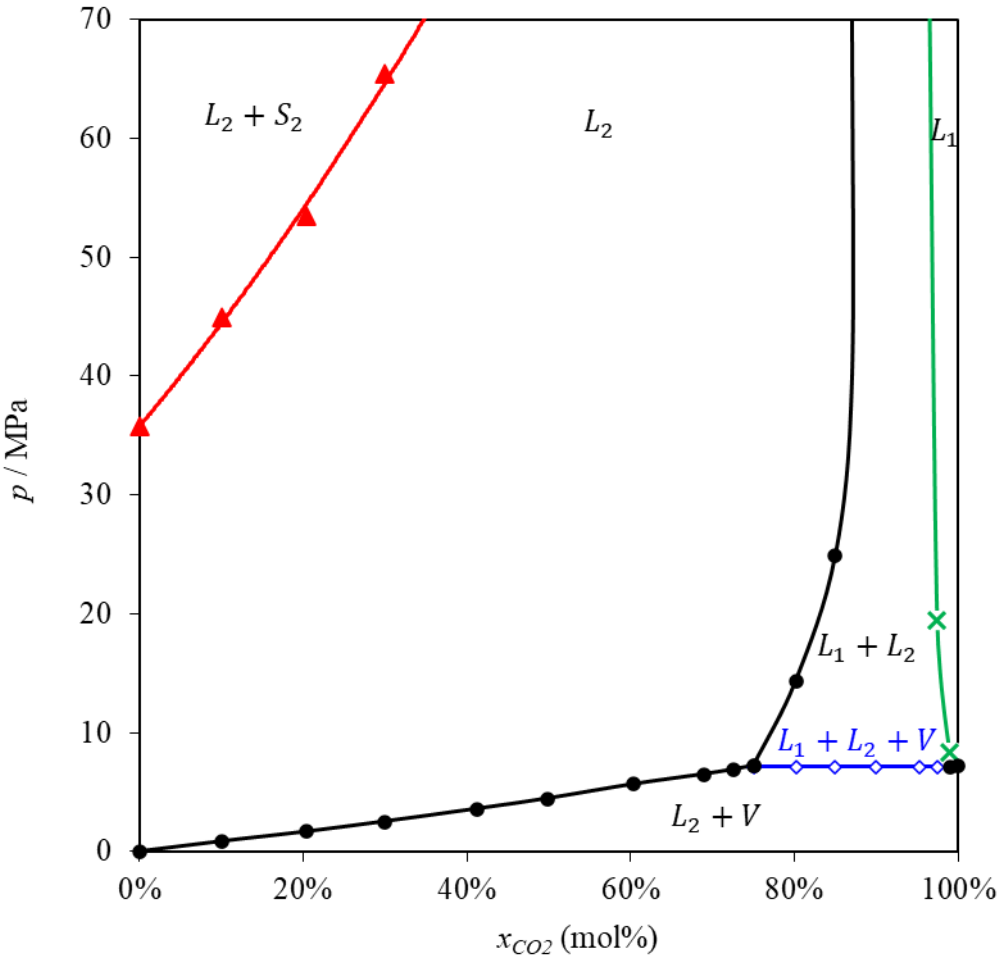

Fig. 16. Isothermal *p*,*x* phase diagram at different temperatures. blue Δ, T = 313.15 K; black ●, T = 323.15 K; □, T = 333.15 K; ◆, T = 343.15 K; ⭘, T = 353.15; ▲, T = 363.15 K.

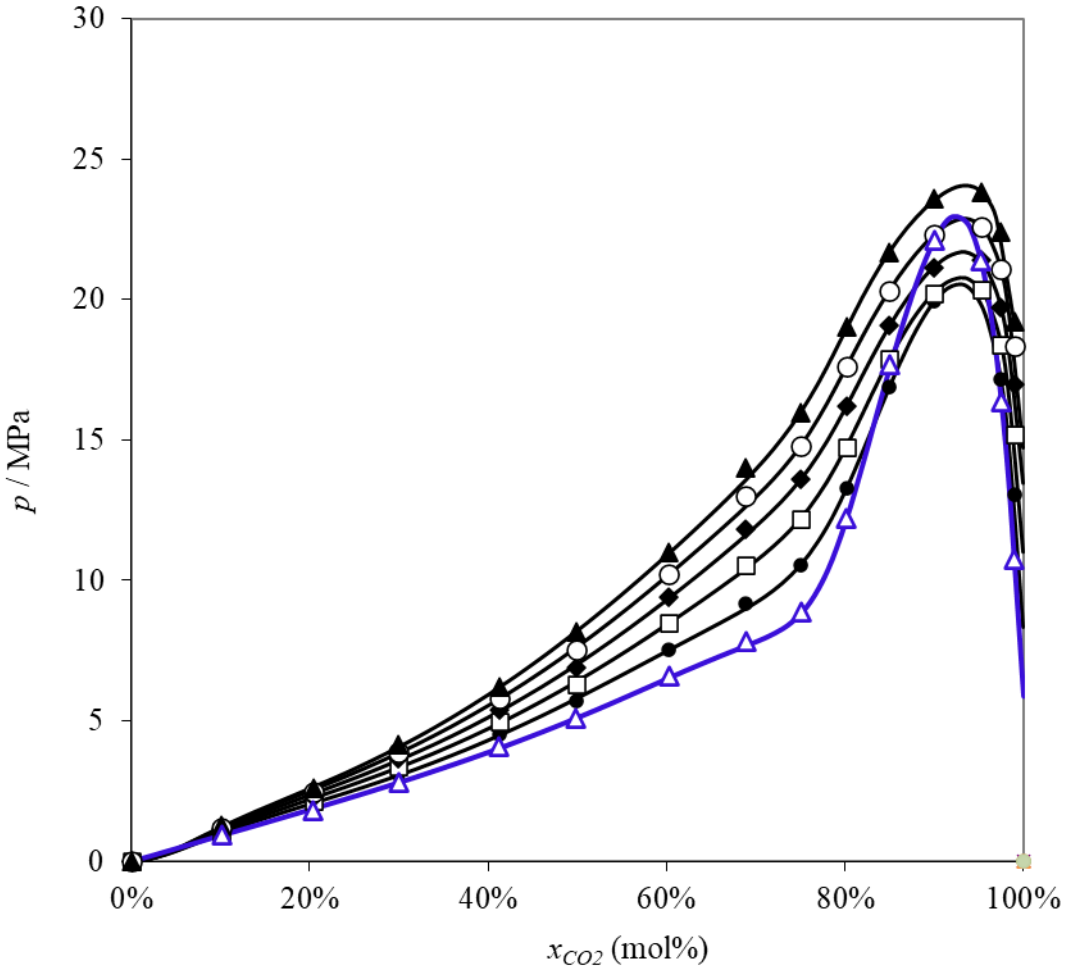

Fig. 17. Isothermal *p,x* phase diagram at T = 323.15 K. black ●, this work; blue ◇, data reported by Pöhler [20]; blue ◆, critical point measured by Pöhler [20]; red ○, blue Δ, critical pressure reported by Scheidgen [13].

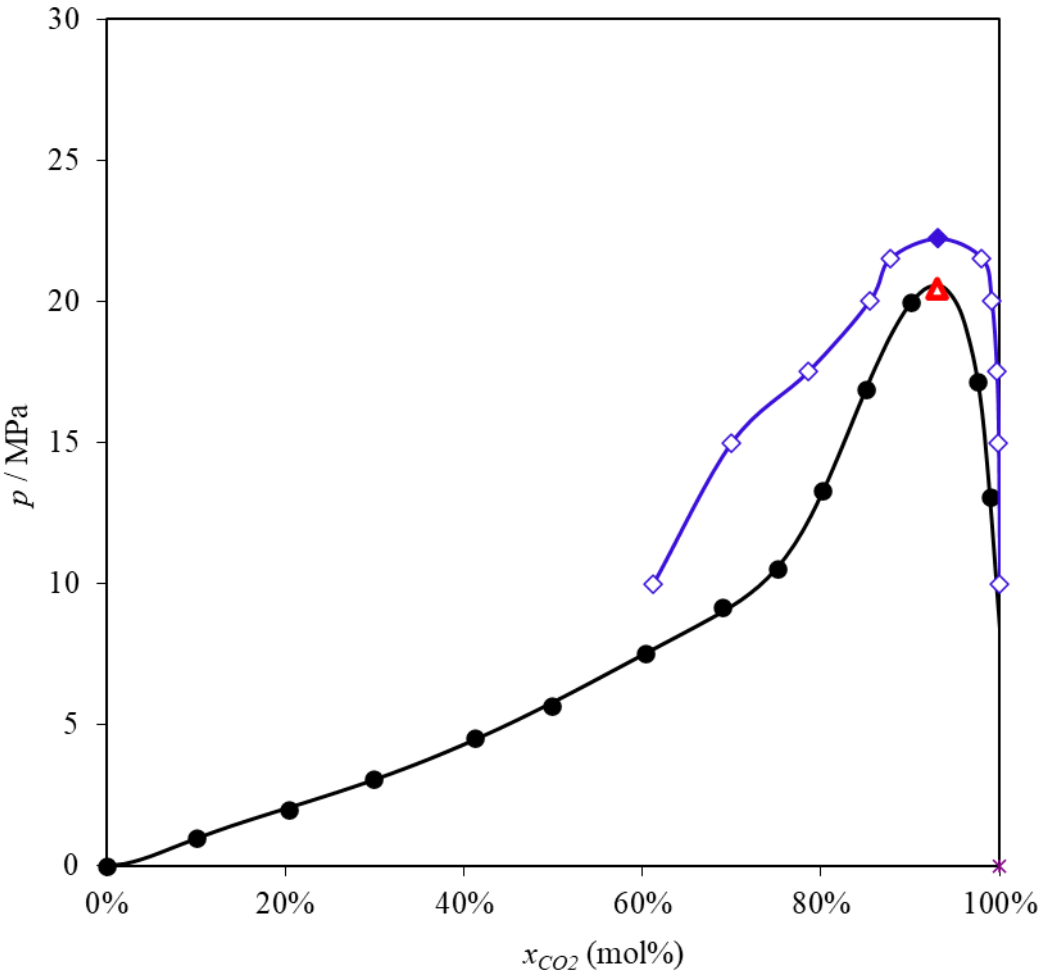

Fig. 18. Isothermal *p,x* phase diagram at T = 353.15 K. black ●, this work; blue ◇, data reported by Pöhler [20]; blue ◆, critical point measured by Pöhler [20]; red ⭘, blue Δ, critical pressure reported by Scheidgen [13].

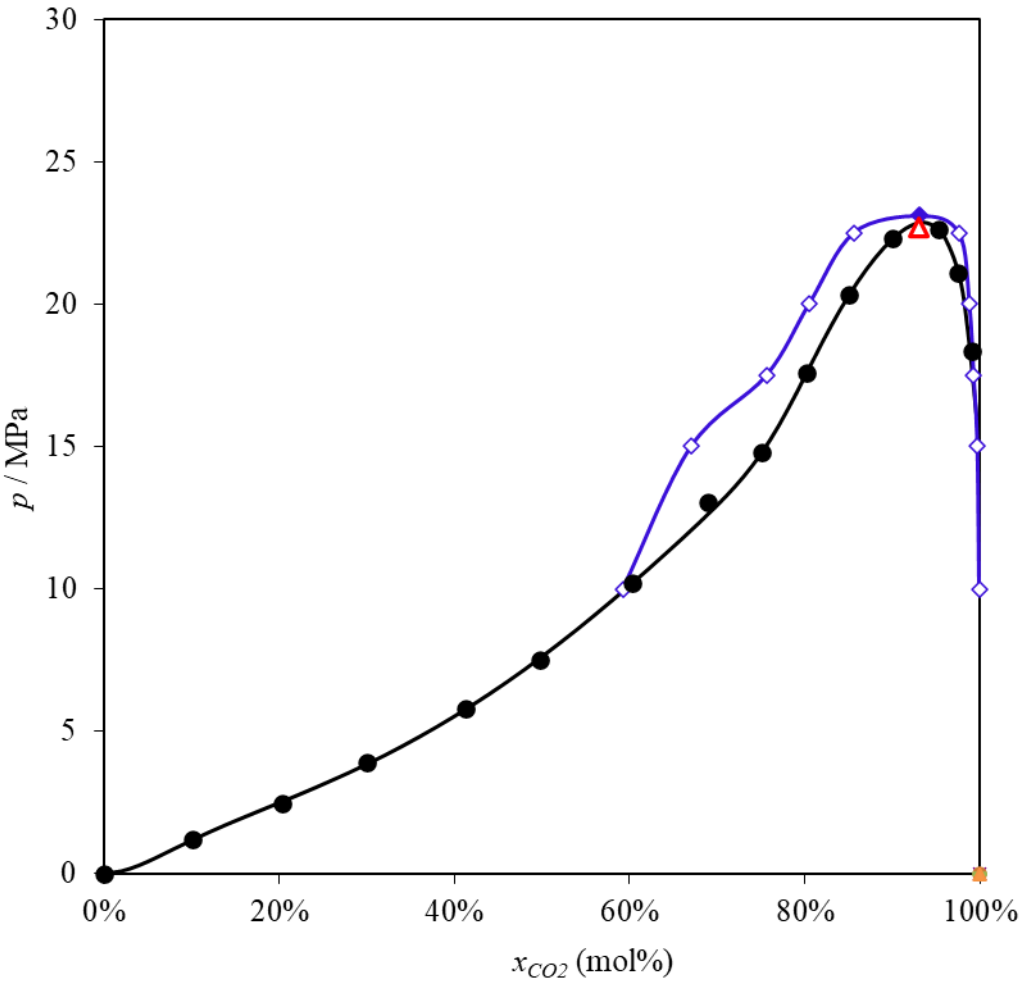

Graphical abstract